TRACTION CONTROL OF ALL-WHEEL-DRIVE INDEPENDENT SUSPENSION MOBILE ROBOTS IN 2D ROUGH TERRAIN

Alexandre F. Barral Silva, barral99@yahoo.com.br
Auderi Vicente Santos, auderi@cetuc.puc-rio.br
Marco Antonio Meggiolaro, meggi@mec.puc-rio.br
Pontifical Catholic University of Rio de Janeiro, Rua Marquês de São Vicente 225 Gávea, Rio de Janeiro, RJ, Brazil

Ney Robinson Salvi dos Reis, salvireis@petrobras.com.br
Centro de Pesquisas e Desenvolvimento (CENPES/PETROBRAS), Cid.Universitaria Q.7, Ilha do Fundão, Rio de Janeiro, RJ, Brazil

Abstract. *Traction control is a critical aspect of mobile robots that need to traverse rough terrain, avoiding excessive slip – which may cause the terrain to collapse locally and trap the robot wheels – and guaranteeing an adequate trajectory and speed control while reducing the power requirements. Traction control of all-wheel-drive robots in rough terrain was originally motivated by space exploration, such as in the case of the Mars Exploration Rovers. However, such technology is also needed in our planet, in particular in the Amazon region. This is the case of the Hybrid Environmental Robot (HER), a 4-wheel-drive mobile robot with independent suspension under development at CENPES/PETROBRAS, which is susceptible to changing terrain conditions, facing slippery soil and steep slopes. In this work, a new traction control scheme is proposed to allow the HER to maintain a desired velocity while minimizing power requirements and slippage, and avoiding motor saturation and loss of wheel contact. Simulations are performed for rough terrain conditions with 2D-profile, considering the general case of different tire-terrain contact angles at each wheel. It is found that the control scheme is able to access in real time the ideal torques required by each independent wheel to maintain the desired speed, even in uneven steep terrain, with minimum power consumption.*

Keywords*: traction control, mobile robot, rough terrain, all-wheel drive*

1. INTRODUCTION

Since 1988 PETROBRAS explores petroleum in Urucu (AM), in the middle of the Amazonian forest. The Urucu plant is the largest Natural Gas Unit in Brazil (UPGN3), with a production of more than six million cubic meters of natural gas per day (Santos, 2007). To safely distribute this production, PETROBRAS is building two gas pipelines, Coari-Manaus (420km long) and Urucu-Porto Velho (550km long). In addition, PETROBRAS is developing a series of robots in the Robotics Laboratory at CENPES to monitor these almost 1000km of pipelines.

Among the robots being developed, there is the Hybrid Environmental Robot (HER), which will be used in the monitoring and data collection of the environment nearby the pipelines. Due to the several types of soils, obstacles and rough terrain that the HER may face in its missions, it is indispensable to have an appropriate traction control that makes it possible to traverse obstacles safely, avoiding wheel slippage and minimizing the power consumption.

The development of traction control for rough terrain has been motivated in the last years, mainly, for space applications (Balaram, 2000). Traction control presents a great number of research works applied to passenger vehicles moving in planar roads (Anwar, 2003). A technique very used by the automotive industry is ABS (Anti-lock Braking System), which consists of using the information of the sliding of each wheel to correct its speed, minimizing skidding (Sakai *et al.*, 1999). Methods based on the ABS system can be derived to be used in the control of mobile robot systems used in space applications (rovers) in rough terrain. However, such methods don't take into account the kinematics and the physical model of the robot, being in this way limited when used in very rough terrain. In addition, the speeds are only altered when the sliding has already happened, therefore the system reacts with a certain delay, generating errors in the robot's location in special if dead reckoning is used.

In Lamon and Siegwart (2005) a method is presented that proposes the minimization of the ratio between the traction and normal forces at each wheel, which are measured with sensors installed at the wheel, to prevent sliding. This method has the advantage of not requiring the knowledge of the soil characteristics and of the robot's speed. Good results were obtained in simulations, however practical experiments were not performed to validate the proposed approach in real situations. In addition, this approach has the inconvenience of the high cost and complexity of the required wheels.

There are also models that are based on obtaining a certain value of optimal sliding (S_{cr}) between the wheels and the soil in order to maximize traction force. The value of S_{cr} depends on the combination of tire/soil, varying considerably for different combinations (Caltabiano *et al.*, 2004). Among the inconveniences of this approach are: the hypothesis of the wheel being flexible and the soil rigid, the need for the knowledge of S_{cr} for each combination of tire/soil, and the need to know the speed of the vehicle and the normal forces acting at each wheel. Burg and Blazevic (1997) presented an approach based on an estimate of S_{cr} that doesn't use the knowledge of the soil characteristics, however it is only valid for flat terrain and it is very susceptible to errors due to variations in the terrain or due to robot's vibrations.

Iagnemma and Dubowsky (2004) presented a traction control method for rough terrain that is not based on torque distribution systems nor on measures of sliding of the wheels. It just uses the properties of the soil and of its geometry to obtain the contact angle between the wheels and the ground. Using this information, the method optimizes the torque at each wheel with the intention of obtaining maximum traction or minimum power consumption, depending on the local level of difficulty/traversability of the terrain. The method presented good results in simulations and in experiments.

The present work presents a traction control scheme for mobile robots in rough terrain that also uses the contact angles between the wheels and the ground. The proposed method, differently from Iagnemma's approach, explicitly considers the robot's dynamic model, including flexible suspensions. It is able to control a desired speed V_d along the longitudinal axis of the robot's chassis, avoiding motor saturation, wheel slip and dynamic instability. In some cases, the control can also minimize the mechanical power required by the robotic system, without the need for heuristically classifying terrains into "easy" or "difficult" as needed in Iagnemma and Dubowsky (2004).

The control methodology is explicitly developed for the 2D case with a generic rough terrain. In the next section, the dynamic model of a 2D mobile robot is presented considering flexible independent suspensions.

2. ANALYTICAL MODELS FOR THE ROBOT AND TERRAIN

The following system model assumes the hypotheses: rigid wheels and soil, inertia of the vehicle concentrated in its center of mass, negligible suspension and wheel inertia compared to the robot chassis', and flexible independent suspensions (modeled as spring-damper systems).

2.1. Terrain model and wheel contact angles

The terrain profile must be provided to the robot, which can be accomplished e.g. using stereo camera systems. The terrain profile curve is modeled as a function formed by the union of discrete (x_i, y_i) points, see Fig. 1. The spacing of these points along the x (horizontal) axis is constant and equal to dx. The coordinate y will be a function of x, in other words, $y_i = f(x_i)$.

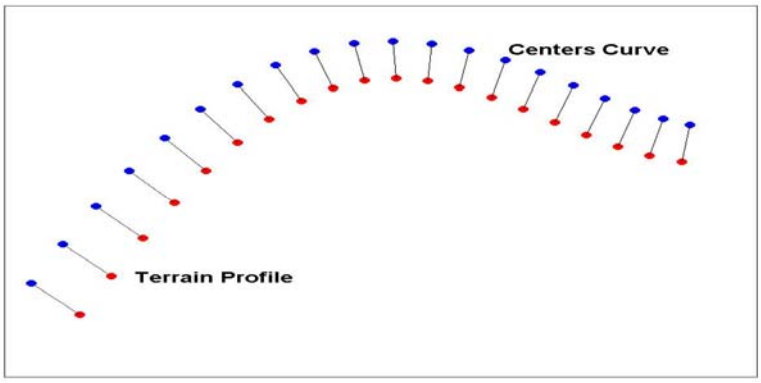

Figure 1. Discrete model of the terrain profile, and associated centers curve

To help in the calculation of the wheel contact point with the terrain at each state of the robotic vehicle, a new curve is generated, denominated *centers curve*. This curve is the geometric locus of the center of a rigid wheel with a known radius r when it is rolled along keeping contact with the terrain. The points (x_{cc}, y_{cc}) of the centers curve, shown in Fig. 1, are generated from the terrain profile points. For each point (x_i, y_i) of the terrain, the point (x_{cc}, y_{cc}), belonging to the line perpendicular to the tangent to the terrain profile and above the terrain at a distance r from the contact point, is calculated, see Fig. 2. Except for a few special degenerate cases where an appropriate mathematical handling must be performed (Silva, 2007), the centers curve for the terrain profile can be expressed as the union of $(x_{cc}, g(x_{cc}))$ points. In other words, the centers curve is a function, and each of its points can be associated to a point (x_i, y_i) of the terrain profile. Thus, to calculate the contact point between a wheel and the terrain, it will be enough to know the coordinates of the center of this wheel, find the closest match in the discretized centers curve, and then correlate it to the terrain profile points, which will be the wheel-terrain contact point. The contact angle γ_i, defined as the angle between the tangent to the terrain profile and the horizontal at the contact point of wheel i ($i = 1$ for the rear wheel and $i = 2$ for the front one) is then obtained from the discrete derivative of (x_i, y_i), see Fig. 2.

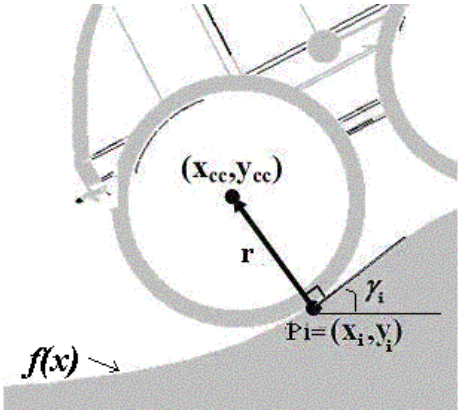

Figure 2. Schematics showing how to obtain the points (x_{cc}, y_{cc}) of the centers curve and the wheel-terrain contact angles γ_i from the terrain profile and wheel radius r

2.2. Dynamic equations of movement

Figure 3 shows a schematic representation of the robot to be analyzed. In this figure, c is the damping coefficient of the robot's suspension, K its stiffness, $C = (x_c, y_c)$ is center of mass of the robot, $C_1 = (x_{c1}, y_{c1})$ and $C_2 = (x_{c2}, y_{c2})$ are the geometric centers of wheels 1 (rear) and 2 (front), and ξ_1 and ξ_2 are the displacements of the suspensions of wheels 1 and 2, respectively. The distance between the wheel centers and the robot center along a line normal to the robot chassis, when the suspension is relaxed, is $h = h_1 = h_2$.

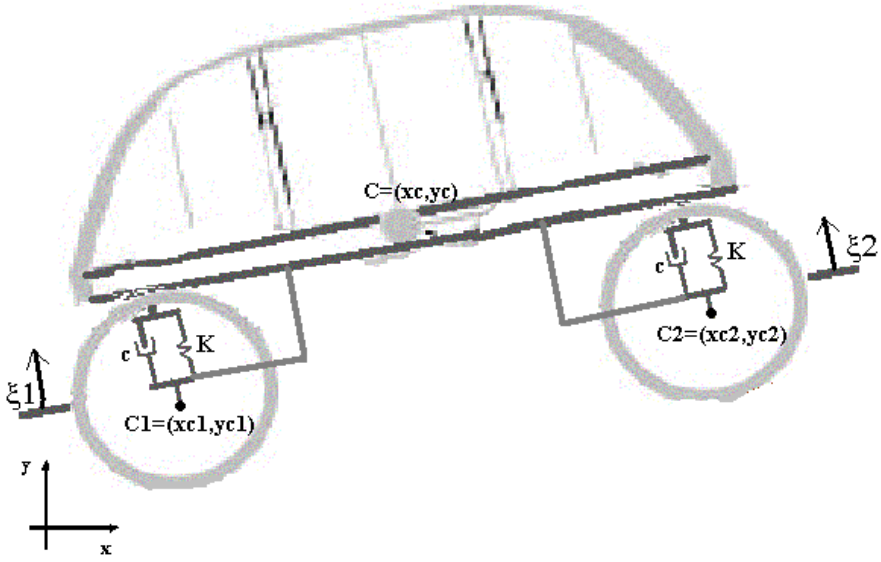

Figure 3. 2D Model of the mobile robot with independent suspensions

From the free body diagram of the robot chassis shown in Fig. 4, and applying Newton-Euler's equations, then

$$\sum F_x = m \cdot \ddot{x}_c \Rightarrow m \cdot \ddot{x}_c = [K \cdot (\xi_1 + \xi_2) + c \cdot (\dot{\xi}_1 + \dot{\xi}_2)] \cdot sin\alpha + (F_{r1} + F_{r2}) \cdot \cos\alpha \quad (1)$$

$$\sum F_y = m \cdot \ddot{y}_c \Rightarrow m \cdot \ddot{y}_c = -[K \cdot (\xi_1 + \xi_2) + c \cdot (\dot{\xi}_1 + \dot{\xi}_2)] \cdot \cos\alpha + (F_{r1} + F_{r2}) \cdot sin\alpha - P \quad (2)$$

$$\sum M_{CM} = I \cdot \ddot{\alpha} \Rightarrow I \cdot \ddot{\alpha} = (K \cdot \xi_1 + c \cdot \dot{\xi}_1) \cdot L_1 - (K \cdot \xi_2 + c \cdot \dot{\xi}_2) \cdot L_2 + F_{r_1} \cdot (h_1 + \xi_1) + F_{r_2} \cdot (h_2 + \xi_2) \quad (3)$$

where m is the total mass and I the moment of inertia of the robot, $\dot{\xi}_i$ is the rate of the displacement in suspension i in the direction normal to the robot chassis, F_{ri} is the internal reaction force of suspension i onto the chassis in its longitudinal direction, P is the system weight, and α is the slope angle of the chassis with respect to the x axis.

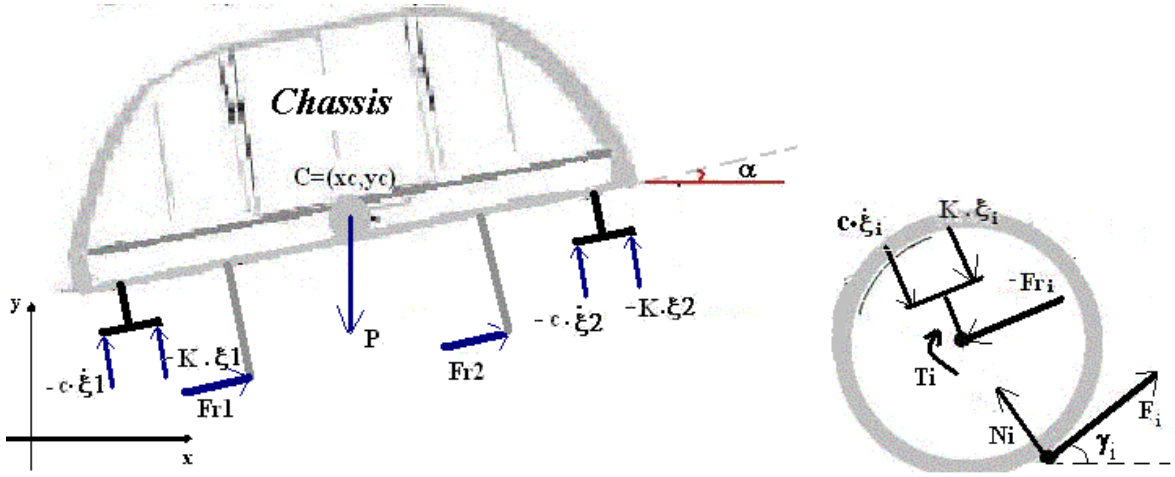

Figure 4. Free body diagrams of the robot chassis and wheel *i*

The free body diagram of each wheel *i* (*i* = 1, 2) is also shown above. Neglecting the wheel inertia, Newton-Euler's equations result in

$$\sum F_x = 0 \Rightarrow -(K\cdot\xi_i + c\cdot\dot{\xi}_i)\cdot sin\alpha - F_{ri}\cdot cos\,\alpha + F_i\cdot cos\,\gamma_i - N_i\cdot sin\gamma_i = 0 \tag{4}$$

$$\sum F_y = 0 \Rightarrow (K\cdot\xi_i + c\cdot\dot{\xi}_i)\cdot cos\,\alpha - F_{ri}\cdot sin\alpha + F_i\cdot sin\gamma_i + N_i\cdot cos\,\gamma_i = 0 \tag{5}$$

$$\sum M_{Ci} = 0 \Rightarrow F_i\cdot r - T_i = 0 \Rightarrow F_i = T_i / r \tag{6}$$

where N_i and F_i are the normal and friction forces between the robot's wheel *i* and the terrain, T_i is the input torque at wheel *i* provided by its motor, and γ_i is the contact angle between the wheel *i* and the terrain.

From Eqs. (4) and (5), the values of N_i and F_{ri} can be obtained, resulting in

$$N_i = F_i\cdot tan(\gamma_i - \alpha) + \frac{(K\cdot\xi_i + c\cdot\dot{\xi}_i)}{cos(\gamma_i - \alpha)} \tag{7}$$

$$F_{ri} = (K\cdot\xi_i + c\cdot\dot{\xi}_i)\cdot tan(\gamma_i - \alpha) + \frac{F_i}{cos(\gamma_i - \alpha)} \tag{8}$$

Substituting the above equations into Eqs. (1-3), then

$$\begin{aligned} m\cdot\ddot{x}_c &= (K\cdot\xi_1 + c\cdot\dot{\xi}_1)\cdot[sin\alpha + \tan(\gamma_1 - \alpha)\cdot\cos\alpha] \\ &+ (K\cdot\xi_2 + c\cdot\dot{\xi}_2)\cdot[sin\alpha + \tan(\gamma_2 - \alpha)\cdot\cos\alpha] + Fat_1\cdot\frac{\cos\alpha}{\cos(\gamma_1 - \alpha)} + Fat_2\cdot\frac{\cos\alpha}{\cos(\gamma_2 - \alpha)} \end{aligned} \tag{9}$$

$$\begin{aligned} m\cdot\ddot{y}_c &= (K\cdot\xi_1 + c\cdot\dot{\xi}_1)\cdot[-\cos\alpha + \tan(\gamma_1 - \alpha)\cdot sin\alpha] \\ &+ (K\cdot\xi_2 + c\cdot\dot{\xi}_2)\cdot[-\cos\alpha + \tan(\gamma_2 - \alpha)\cdot sin\alpha] + Fat_1\cdot\frac{sin\alpha}{\cos(\gamma_1 - \alpha)} + Fat_2\cdot\frac{sin\alpha}{\cos(\gamma_2 - \alpha)} - P \end{aligned} \tag{10}$$

$$\begin{aligned} I\cdot\ddot{\alpha} &= (K\cdot\xi_1 + c\cdot\dot{\xi}_1)\cdot[L_1 + \tan(\gamma_1 - \alpha)\cdot(h_1 + \xi_1)] - (K\cdot\xi_2 + c\cdot\dot{\xi}_2)\cdot[L_2 + \tan(\gamma_2 - \alpha)\cdot(h_2 + \xi_2)] \\ &+ Fat_1\cdot\frac{(h_1 + \xi_1)}{\cos(\gamma_1 - \alpha)} + Fat_2\cdot\frac{(h_2 + \xi_2)}{\cos(\gamma_2 - \alpha)} \end{aligned} \tag{11}$$

The values of ξ_i and $\dot{\xi}_i$ are calculated from the current system state ($x_c, y_c, \alpha, \dot{x}_c, \dot{y}_c, \dot{\alpha}$) and from the coordinates of the center of wheel *i*, (x_{ci}, y_{ci}), which are known from the terrain profile, resulting in

$$\xi_i = -(x_c - x_{ci})\cdot sin\alpha + (y_c - y_{ci})\cdot\cos\alpha \tag{12}$$

$$\dot{\xi}_i = -(\dot{x}_c - \dot{x}_{ci})\cdot sin\alpha + (\dot{y}_c - \dot{y}_{ci})\cdot\cos\alpha - [(x_c - x_{ci})\cdot\cos\alpha + (y_c - y_{ci})\cdot sin\alpha]\cdot\dot{\alpha} \tag{13}$$

where $[\dot{x}_{ci}, \dot{y}_{ci}]^T$ is the velocity vector of the center of wheel *i*.

Since the inertia of the wheels and suspensions is neglected, the suspension can never suffer elongation. Thus, Eqs. (12-13) are only valid if $\xi_i < 0$, with the suspension *i* under compression, otherwise $\xi_i = \dot{\xi}_i = 0$. Thus, whenever Eq. (13) is valid, then the velocity components of the center of wheel *i* will be related by

$$\dot{y}_{ci} = \tan\gamma_i \cdot \dot{x}_{ci} \tag{14}$$

The speed of the center of wheel *i* in the longitudinal direction to the chassis is

$$V_{ci}^{L} = V_c^{L} + (h_i + \xi_i) \cdot \dot{\alpha} \tag{15}$$

where

$$V_{ci}^{L} = \dot{x}_{ci} \cdot \cos\alpha + \dot{y}_{ci} \cdot sin\alpha \tag{16}$$

$$V_c^{L} = \dot{x}_c \cdot \cos\alpha + \dot{y}_c \cdot sin\alpha \tag{17}$$

Substituting Eqs. (16-17) into Eq. (15) and using Eq. (14),

$$\dot{x}_{ci} = \frac{\dot{x}_c \cdot \cos\alpha + \dot{y}_c \cdot sin\alpha + (h_i + \xi_i) \cdot \dot{\alpha}}{(\cos\alpha + \tan\gamma_i \cdot sin\alpha)} \tag{18}$$

$$\dot{y}_{ci} = \tan\gamma_i \cdot \left(\frac{\dot{x}_c \cdot \cos\alpha + \dot{y}_c \cdot sin\alpha + (h_i + \xi_i) \cdot \dot{\alpha}}{(\cos\alpha + \tan\gamma_i \cdot sin\alpha)} \right) \tag{19}$$

Substituting Eqs. (18-19) into Eq. (11) it is possible to obtain $\dot{\xi}_i$ as a function of the current system state and the coordinates of the center of wheel *i*,

$$\begin{aligned} \dot{\xi}_i = {} & [\tan(\alpha - \gamma_i) \cdot \cos\alpha - sin\alpha] \cdot \dot{x}_c + [\tan(\alpha - \gamma_i) \cdot sin\alpha - \cos\alpha] \cdot \dot{y}_c \\ & + [(h_i + \xi_i) \cdot \tan(\alpha - \gamma_i) - (x_c - x_{ci}) \cdot \cos\alpha - (y_c - y_{ci}) \cdot sin\alpha] \cdot \dot{\alpha} \end{aligned} \tag{20}$$

The deformations and rates of deformation of the suspensions of both wheels can be then obtained from Eqs. (12) and (20). Substituting these values into Eqs. (9-11) above, it can be seen that the system accelerations will be a function of only the friction forces acting between the wheels and the terrain (F_1 and F_2, which are controllable from the motor torques) and of other known variables. These forces can then be chosen at each time step to optimize a given system characteristics, which will be addressed next.

3. THE PROPOSED TRACTION CONTROL

The proposed traction control scheme has the objective to provide wheel torques that will let the robot surpass obstacles in rough terrain while keeping a constant desired speed V_d of its center of mass in the longitudinal direction to the chassis. The control must also guarantee contact of all wheels to the ground and avoid slippage and motor saturation. If more than one combination of motor torques is able to accomplish the above requirements, then the proposed control will also find the solution that minimizes the system power consumption. The control technique is described next.

3.1. Calculation of the acceptable wheel traction forces

The control methodology first searches for motor torques that can generate appropriate traction (friction) forces F_1 and F_2, at the same time avoiding motor saturation, slippage and loss of wheel contact. These conditions can be written through the following inequalities:

a) $|F_1| \leq F_{sat1}$, to avoid saturation of the motor of wheel 1, where F_{sat1} is the motor saturation torque divided by *r*;
b) $|F_2| \leq F_{sat2}$, to avoid saturation of the motor of wheel 2;
c) $N_1 > 0$, condition for wheel 1 not to lose ground contact;
d) $N_2 > 0$, condition for wheel 2 not to lose ground contact;
e) $|F_1| \leq \mu \cdot N_1$, to avoid wheel 1 slippage, where μ is the wheel-terrain static friction coefficient; and
f) $|F_2| \leq \mu \cdot N_2$, to avoid wheel 2 slippage.

Substituting i = 1, 2 into Eq. (7), then conditions c) and d) result in:

$$N_1 = F_1 \cdot tan(\gamma_1 - \alpha) + \frac{(K \cdot \xi_1 + c \cdot \dot{\xi}_1)}{cos(\gamma_1 - \alpha)} > 0 \quad \text{and} \quad N_2 = F_2 \cdot tan(\gamma_2 - \alpha) + \frac{(K \cdot \xi_2 + c \cdot \dot{\xi}_2)}{cos(\gamma_2 - \alpha)} > 0 \tag{21}$$

It can be seen that, for a given system state, all conditions above are bounded by vertical or horizontal lines in the $F_1 \times F_2$ plane. Therefore, the intersection of all regions above can only result in either a rectangular region D or an empty set, see Fig. 5.

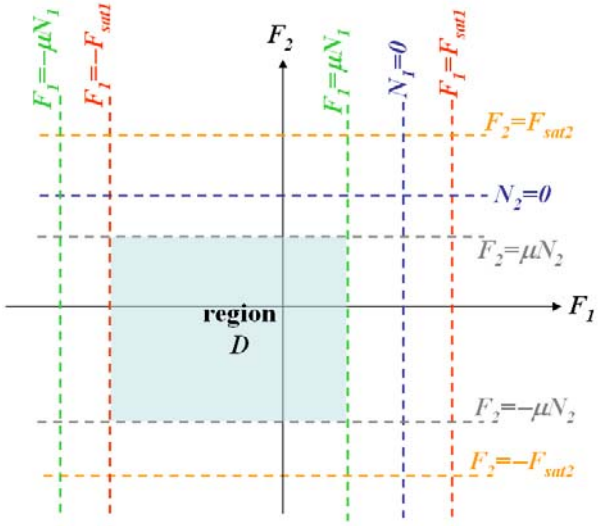

Figure 5. Region D is the locus of the possible (F_1, F_2) combinations that satisfy all conditions a) through f)

3.2. Speed control law

One of the objectives of the proposed control is to guarantee that the speed V_L of the robot's center of mass along the longitudinal direction to the chassis is equal to a desired speed V_d, therefore it is desired that

$$V_L = V_d \Rightarrow \dot{x}_c \cdot cos\,\alpha + \dot{y}_c \cdot sin\alpha = V_d \tag{22}$$

The longitudinal velocity V_L can be calculated at an instant t_f from its value ${}^0V_L$ at an initial instant t_0 and the acceleration $a_L(t)$ of the center of mass in the longitudinal direction

$$V_L = {}^0V_L + \int_{t0}^{tf} a_L \cdot dt \tag{23}$$

The acceleration a_L can be controlled through the wheel torques, which in turn control the wheel-terrain friction forces. Being a first order system, as seen in Eq. (23), proportional control is satisfactory. Considering a proportional gain K_p for the error between the desired and actual longitudinal speeds, the following control law is proposed:

$$a_L := K_p \cdot (V_d - V_L) \tag{24}$$

The acceleration a_L can be calculated from the center of mass acceleration components and the angle α,

$$a_L = \ddot{x}_c \cdot \cos\alpha + \ddot{y}_c \cdot sin\alpha \tag{25}$$

From Eqs. (9-10), the acceleration a_L can be written as a function of the friction forces F_1 and F_2 and of parameters η_1, η_2 and a_0 which are known for a given state,

$$a_L = \eta_1 \cdot F_1 + \eta_2 \cdot F_2 + a_0 \tag{26}$$

where

$$\eta_1 \equiv \frac{1}{m \cdot \cos(\gamma_1 - \alpha)}, \quad \eta_2 \equiv \frac{1}{m \cdot cos(\gamma_2 - \alpha)} \tag{27}$$

$$a_0 \equiv \zeta_1 \cdot \cos\alpha + \zeta_2 \cdot sin\alpha - P \cdot sin\alpha / m \tag{28}$$

$$\zeta_1 \equiv \frac{(K\cdot\xi_1 + c\cdot\dot{\xi}_1)\cdot[sin\alpha + \tan(\gamma_1-\alpha)\cdot\cos\alpha] + (K\cdot\xi_2 + c\cdot\dot{\xi}_2)\cdot[sin\alpha + \tan(\gamma_2-\alpha)\cdot\cos\alpha]}{m} \tag{29}$$

$$\zeta_2 \equiv \frac{(K\cdot\xi_1 + c\cdot\dot{\xi}_1)\cdot[-\cos\alpha + \tan(\gamma_1-\alpha)\cdot sin\alpha] + (K\cdot\xi_2 + c\cdot\dot{\xi}_2)\cdot[-\cos\alpha + \tan(\gamma_2-\alpha)\cdot sin\alpha]}{m} \tag{30}$$

Eqs. (24-26) result in:

$$\eta_1\cdot F_1 + \eta_2\cdot F_2 = K_p\cdot(V_d - V_L) - a_0 \tag{31}$$

The values of F_1 and F_2 that satisfy the above equation will generate a straight line S in the $F_1 \times F_2$ plane. This line represents all combinations of friction forces that are able to perform speed control for a desired V_d. Thus, the intersection set Γ between the region D and the straight line S will return all possible combinations that, besides controlling the robot speed, satisfy all conditions a) through f) described before.

When Γ is an empty set (i.e. S does not cross region D), then the proposed technique won't be able to perform speed control without violating the conditions, which are more important since they're related to the system integrity. In this case, the control algorithm looks for the point $P = (F_1, F_2)$ inside region D that will lead to the acceleration a_e closest to the desired value a_L from Eq. (24), see Fig. 6(a). Since iso-acceleration lines in the $F_1 \times F_2$ plane are always straight lines, as seen from Eq. (26), one of the vertices of the rectangle D will always be the closest point to the external iso-acceleration line associated with a_L. It is then enough to calculate the longitudinal accelerations associated to the four vertices of D, and choose the one closest to a_L, e.g. the point P in Fig. 6(a).

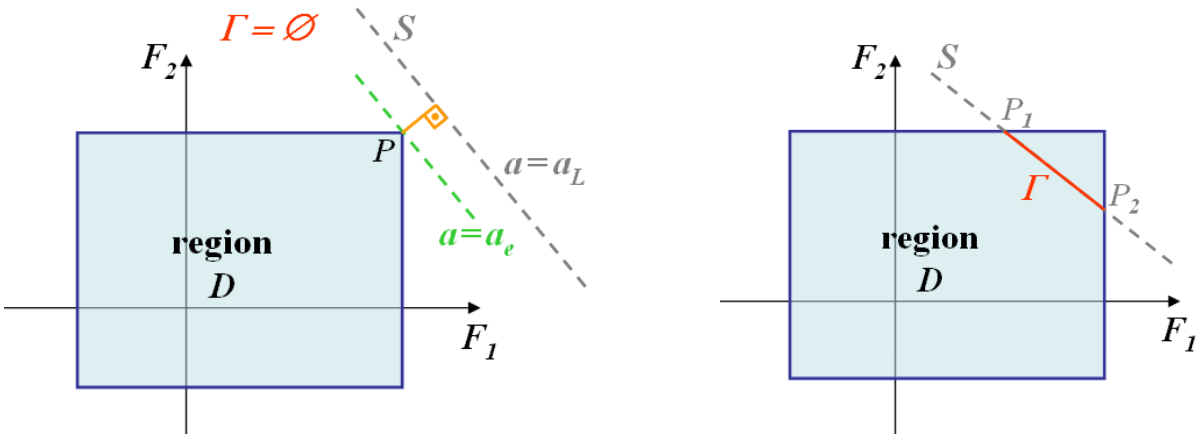

Figure 6. (a) Point P closest to S when Γ is empty and (b) definition of the Γ set in the $F_1 \times F_2$ plane

On the other hand, if Γ is not empty, then it will be either a vertex from D or a straight line segment P_1-P_2, see Fig. 6(b). In the latter case, there will be infinite points $(F_1, F_2) \in \Gamma$ that could be chosen to control the robot's longitudinal velocity guaranteeing conditions a) through f). Another optimization criterion can then be used to choose a point in Γ. The minimization of the robot power consumption is chosen in this work, as described next.

3.3. Minimization of the system power consumption

The power dissipated by the wheel motors can be divided into two parts, one due to the mechanical output work at the motor shaft, and another due to power losses (such as in the Joule effect in DC motors). Assuming that the motor efficiency is high (e.g. a DC motor with low internal electric resistance and low no-load currents), then the second part is neglected, resulting in a total required power for both wheels

$$P_T = |T_1\cdot\omega_1| + |T_2\cdot\omega_2| \tag{32}$$

where T_i is the output torque at wheel i, in N·m, and ω_i its angular velocity, in rad/s. The above expression assumes that the robot does not have regenerative braking, i.e., it does not recover energy from the braking process (which, however, would be possible when using DC motors, as the batteries could be recharged when T_i and ω_i have opposite signs).

Assuming no slip between the wheels and motor shafts (due to clutches, e.g.), and neglecting the wheel inertia, then T_i is equal to the friction force F_i multiplied by the wheel radius r. Also, assuming the proposed control won't allow wheel slip, then $|\omega_i|$ is equal to the speed $|V_{ci}|$ of the center of wheel i divided by r. Equation (32) becomes

$$P_T = |F_1 \cdot r \cdot V_{c1} / r| + |F_2 \cdot r \cdot V_{c2} / r| = |F_1| \cdot |V_{c1}| + |F_2| \cdot |V_{c2}| \tag{33}$$

For a desired longitudinal speed V_d of the robot center of mass, the speeds of the wheel centers can be calculated by

$$|V_{ci}| = \left| \frac{V_d + (h_i + \xi_i) \cdot \dot{\alpha}}{\cos(\gamma_i - \alpha)} \right| \tag{34}$$

From Eqs. (33-34), the total power required by the system is a function of the parameters ∇_1 and ∇_2, which are constant for a given system state and desired speed, and of the friction forces F_1 and F_2

$$P_T = |F_1| \cdot \nabla_1 + |F_2| \cdot \nabla_2 \tag{35}$$

$$\nabla_1 \equiv \left| \frac{V_d + (h_1 + \xi_1) \cdot \dot{\alpha}}{\cos(\gamma_1 - \alpha)} \right| \quad \text{and} \quad \nabla_2 \equiv \left| \frac{V_d + (h_2 + \xi_2) \cdot \dot{\alpha}}{\cos(\gamma_2 - \alpha)} \right| \tag{36}$$

From Eq. (35), the locus of the points with same power in the $F_1 \times F_2$ plane would have a diamond shape, centered at the origin. Therefore, the power consumption minimization problem could be geometrically regarded as finding the smallest diamond that would intersect with the segment Γ. Clearly, there are four basic cases: the intersection point that minimizes power could be point P_1, P_2, or the intersection of Γ with the F_1 axis or with the F_2 axis, see Fig. 7.

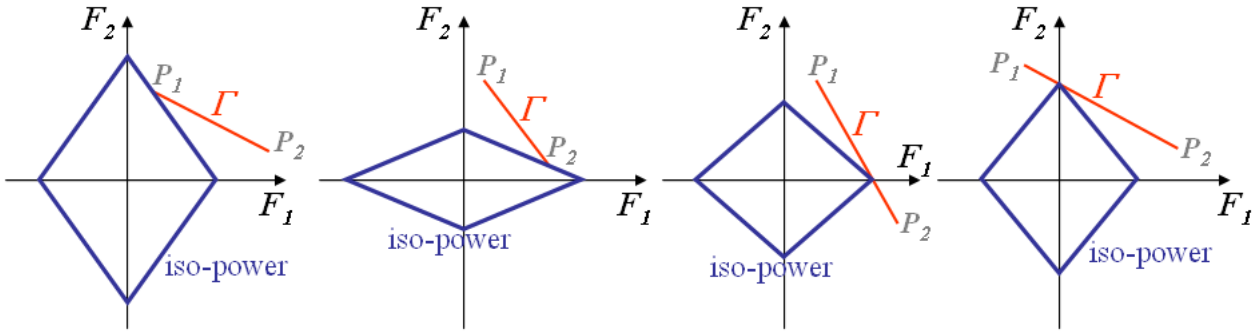

Figure 7. Intersection points between Γ and the smallest iso-power diamond for the 4 basic cases

Note that if Γ is parallel to any side of the diamond, then there may be an infinite number of solutions. But, in any case, at least one of the solutions shown in Fig. 7 is valid. Thus it is enough for the algorithm to calculate the power at points P_1, P_2, and at the intersection of Γ with the F_1 and F_2 axes (if it intersects either axis), and choose the solution that results in minimum power. The resulting optimized F_1 and F_2 values are used to calculate the associated wheel torques, which are then commanded to the motors. In this way, the robot is able to control its speed in rough terrain while guaranteeing wheel-terrain contact and avoiding slippage and motor saturation, minimizing power consumption when possible. In the next section, the proposed approach is verified through simulations.

4. RESULTS

Simulations are performed using real parameters taken from the second prototype of the Hybrid Environmental Robot (HER), namely $m = 120$kg, $I = 15.22$kg·m^2, $F_{sat1} = F_{sat2} = 320$N, $r = 0.3$m, $L_1 = L_2 = 0.7$m, $h_1 = h_2 = 0.125$m, $K = 10^5$N/m and $c = 4.8 \cdot 10^3$kg/s. Also, g = 9.8m/s^2, and the wheel-terrain friction coefficient is assumed as $\mu = 0.5$.

The proposed control is compared with traditional velocity control (TVC) with gravity compensation. TVC assumes that the terrain below the wheels is approximately flat, therefore the wheel-terrain contact angles are equal to the chassis angle, $\gamma_1 = \gamma_2 = \alpha$. In this special case, Eq. (31) would become

$$F_1 + F_2 = m \cdot K_p \cdot (V_d - V_L) + P \cdot \sin\alpha \tag{37}$$

Note that, on an ideal flat terrain, only the sum of the friction forces F_1 and F_2 matters, not their individual values (as long as such values do not cause slippage, motor saturation or loss of wheel contact, which are not modeled in the

TVC). TVC then distributes evenly the torque to both motors, resulting in the same forces F_1 and F_2. The TVC law with gravity compensation is then

$$F_1 = F_2 := [m \cdot K_p \cdot (V_d - V_L) + P \cdot \sin\alpha]/2 \tag{38}$$

The same proportional gain K_p is used for the proposed traction control and for the TVC, providing a fair comparison. In fact, Eqs. (37-38) prove that both control techniques should result in the same response for flat terrains with small slopes.

Figure 8 shows the terrain profiles considered in the simulations. All simulations assume zero initial robot velocity. For the flat terrain simulation, K_p is chosen as $490s^{-1}$. This gain value is found appropriate for several terrains with average 30 degree slopes. Higher values could be used without compromising the validity of the simulations, because motor saturation is included in the model. For the rough terrain simulation, which has higher slopes as seen in Fig. 8(b), the gain is doubled, i.e. K_p is chosen as $980s^{-1}$. An estimate of the highest expected slopes in the terrain is useful to calibrate K_p, however if this information is not available then it can be estimated from the maximum slope the robot would be able to climb without tipping over.

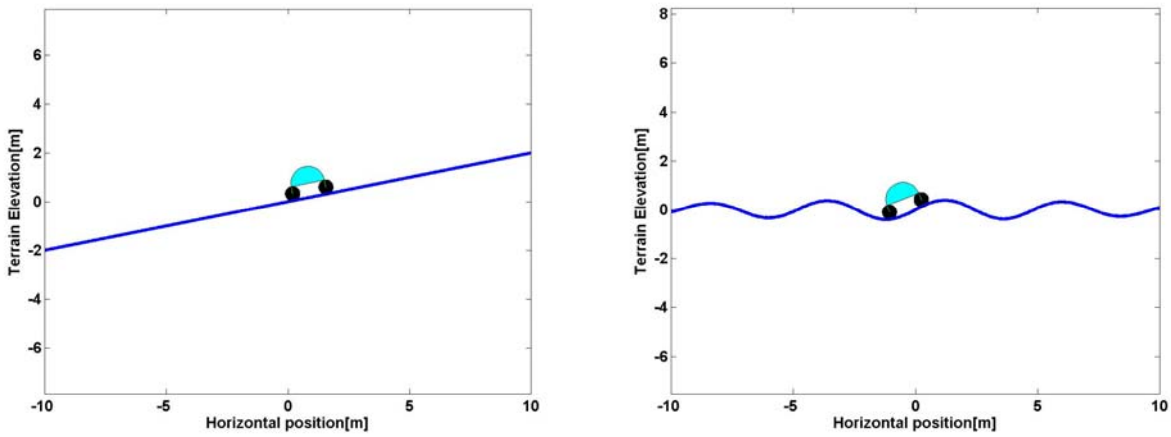

(a) (b)

Figure 8. Terrain profiles used in simulations for: (a) flat terrain; (b) rough terrain.

The results for the flat terrain simulations are shown in Fig. 9. This figure shows the robot's longitudinal speed from traction control and TVC. The proposed traction control performs much better than TVC, settling to the desired speed V_d = 1m/s in less than 1s instead of more than 4s.

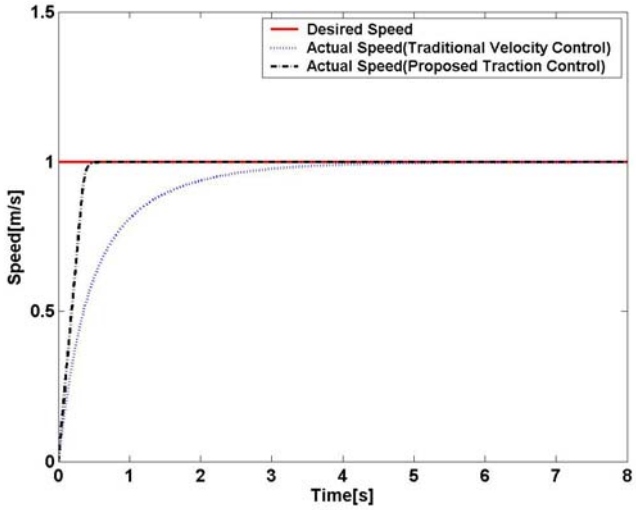

Figure 9. Longitudinal speed of the robot on flat terrain with traction control and with TVC

The results for the rough terrain simulations are shown in Fig. 10. This figure shows the robot's longitudinal speed from traction control and TVC. The advantages of the proposed traction control can be clearly seen, settling to the

desired speed V_d = 1m/s in approximately 0.5s, without oscillations. TVC, on the other hand, doesn't converge to V_d, presenting oscillations with high overshoot (approximately 40%) excited by the wavy terrain profile. Note that even gravity compensation is not enough in the TVC to avoid such oscillations, because of the hypothesis of flat terrain ($\gamma_1 = \gamma_2 = \alpha$) used in this compensation. Indeed, it can be clearly seen in Fig. 8(b) that the slope α of the robot chassis can be very different from the wheel-terrain contact angles γ_1 and γ_2 as the vehicle moves along the wavy path.

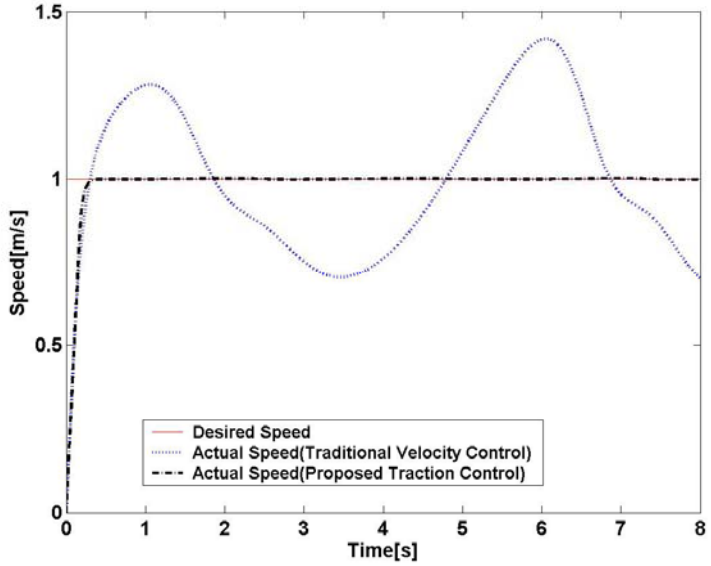

Figure 10. Longitudinal speed of the robot on rough terrain with traction control and with TVC

5. CONCLUSIONS

In this work, a novel traction control methodology was proposed to achieve desired speeds in rough terrain, while guaranteeing wheel-terrain contact and avoiding slippage and motor saturation. When possible, power consumption was also minimized. The methodology explicitly considers the different contact angles at each wheel and the dynamic interaction between the vehicle and the terrain. Simulations demonstrated the effectiveness of the proposed traction control for flat and rough terrain, managing to reach the desired speeds much faster than traditional velocity control techniques with gravity compensation under similar conditions. The proposed approach converges with low power requirements even for very rough terrain, where traditional techniques aren't able to effectively control the robot speed.

6. REFERENCES

Balaram, J., 2000, "Kinematic state estimation for a Mars Rover", Robotica, Vol.18, pp. 251-262.

Burg, J. and Blazevic, P., 1997, "Anti-Lock Braking and Traction Control Concept for All-Terrain Robotic Vehicles**",** in IEEE International Conference on Robotics and Automation, Albuquerque, USA.

Caltabiano, D., Ciancitto, D. and Muscato, G., 2004, "Experimental Results on a Traction Control Algorithm for Mobile Robots in Volcano Environment**",** in IEEE International Conference on Robotics and Automation, New Orleans, USA.

Iagnemma, K. and Dubowsky, S., 2004, "Mobile Robot in Rough Terrain: Estimation, Motion Planning, and Control with Application to Planetary Rovers", Berlim: Springer, 110p.

Lamon, P. and Siegwart, R., 2005, "Wheel Torque Control in Rough Terrain: Modeling and Simulation", in IEEE International Conference on Robotics and Automation, Barcelona, Spain.

Sakai, S., Sado, H. and Hori, Y., 1999, "Motion Control in an Electric Vehicle with Four Independently Driven In-Wheel Motors**",** IEEE/ASME Transactions on Mechatronics, Vol.4, No. 1, pp. 9-16.

Santos, A.V., 2007, "Projeto e Controle de Estabilidade de um Sistema Robótico Anfíbio para Sensoriamento Remoto**",** M.Sc. Thesis, Mech. Eng. Dept., Pontifical Catholic University of Rio de Janeiro, 120p, in Portuguese.

Silva, A.F.B., 2007, "Modelagem de Sistemas Robóticos Móveis para Controle de Tração em Terrenos Acidentados**",** M.Sc. Thesis, Mech. Eng. Dept., Pontifical Catholic University of Rio de Janeiro, 126p, in Portuguese.

7. RESPONSIBILITY NOTICE

The authors are the only responsible for the printed material included in this paper.